

# Majorana Fermion Induced Non-local Current Correlations in Spin-orbit Coupled Superconducting Wires

Jie Liu<sup>1,\*</sup>, Fuchun Zhang<sup>1</sup>, and K. T. Law<sup>2†</sup>

<sup>1</sup> Department of Physics, and Center of Theoretical and Computational Physics,  
The University of Hong Kong, Hong Kong, China and

<sup>2</sup> Department of Physics, Hong Kong University of Science and Technology, Clear Water Bay, Hong Kong, China

Recent observation of zero bias conductance peaks in semiconductor wire/superconductor heterostructures has generated great interest, and there is a hot debate on whether the observation is associated with Majorana fermions (MFs). Here we study the local and crossed Andreev reflections in a junction of two normal leads and a sandwiched superconductor-semiconductor wire with two spatially separated but strongly coupled MF end states. The conductance and Fano factors of such a device are sharply different from the topologically trivial case even in the presence of disorder, and can hence be used to identify MFs unambiguously.

PACS numbers: 74.45+c, 74.20.Fg, 74.78.Na

**Introduction** — Recent proposals suggest that Majorana fermions (MFs) can appear as zero energy end states in superconductors constructed by inducing superconductivity on semiconductor wires with Rashba spin-orbit coupling [1–7]. Remarkably, several experimental groups [8–10] recently reported the observation of zero bias conductance peaks (ZBCPs) in Andreev reflection experiments from a normal lead to the end of the aforementioned semiconductor/superconductor heterostructure. These ZBCPs were possibly due to the MF induced Andreev reflection [11, 12]. However, the origin of these ZBCPs remains a subject of debate [13–19].

In this work, instead of studying MF induced local Andreev reflection as done in previous works [13–19], we explore the non-local properties of MFs. Since each MF has only half the degrees of freedom of a Dirac fermion and two spatially separated MFs can form a non-local Dirac fermion, such non-local Dirac fermions can induce non-trivial current-current correlations between two spatially separated normal leads which are coupled to the two MFs. To be specific, an experimental setup depicted in Fig.1a is studied, in which two normal leads are attached to the two ends of an s-wave superconductor with Rashba spin-orbit coupling in the presence of a magnetic field parallel to the wire.

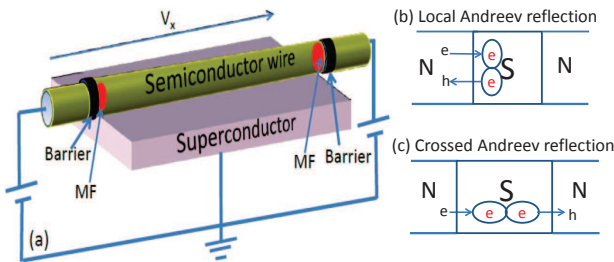


FIG. 1: (a) A schematic setup of experiment, two normal leads are coupled to the two ends of a superconductor which supports MFs. (b) A local Andreev reflection process. An electron from one lead is reflected as a hole in the same lead. (c) A crossed Andreev reflection process. An electron from one lead is reflected as a hole in another lead and a Cooper pair is injected into the superconductor.

When the wire is in the topological regime with MF end states and if the MF end states from the two ends of the wire are coupled, local Andreev reflection processes (as depicted in Fig.1b) can be suppressed and the MF end states induce crossed Andreev reflections, in which an electron from one lead is reflected as a hole in a different lead (as depicted in Fig.1c). Therefore, each normal lead tunnels one electron into the superconductor in each tunnelling event. As a result, the Fano factor, which is the ratio of the shot noise of the current and the average tunnelling current, is  $e$  in the topological regime. On the other hand, the Fano factor which measures the charge transfer of each tunnelling event, is  $2e$  in the topologically trivial regime when local Andreev reflection processes dominate. Therefore, the measurement of the shot noise can be used to distinguish between the topological and non-topological regimes of the wire unambiguously.

It is important to note that an experimental setup similar to Fig.1a has been fabricated recently [10, 20]. The shot noise of leads of the set up is measured [20]. However, the experiment focused only on the trivial regime with zero external magnetic field and the strong magnetic field regime where the proximity gap is suppressed.

**Model and Formalism** — To model the quasi-one dimensional s-wave superconductor with Rashba spin-orbit coupling as shown in Fig.1a, we use the following tight-binding model [7, 13] with  $N_x$  and  $N_y$  sites in the  $x$  and  $y$  directions respectively:

$$\begin{aligned}
 H_{q1D} = & \sum_{\mathbf{R}, \mathbf{d}, \alpha} -t(\psi_{\mathbf{R}+\mathbf{d}, \alpha}^\dagger \psi_{\mathbf{R}, \alpha} + h.c.) - \mu \psi_{\mathbf{R}, \alpha}^\dagger \psi_{\mathbf{R}, \alpha} \\
 & + \sum_{\mathbf{R}, \mathbf{d}, \alpha, \beta} -iU_R \psi_{\mathbf{R}+\mathbf{d}, \alpha}^\dagger \hat{z} \cdot (\vec{\sigma} \times \mathbf{d})_{\alpha\beta} \psi_{\mathbf{R}, \beta} + h.c. \\
 & + \sum_{\mathbf{R}, \alpha, \beta} \psi_{\mathbf{R}, \alpha}^\dagger [(V_x \sigma_x)_{\alpha\beta} + V_{\text{imp}}(\mathbf{R}) \delta_{\alpha\beta}] \psi_{\mathbf{R}, \beta} \\
 & + \sum_{\mathbf{R}, \alpha} \Delta \psi_{\mathbf{R}, \alpha}^\dagger \psi_{\mathbf{R}, -\alpha}^\dagger + h.c.
 \end{aligned} \tag{1}$$

Here,  $\mathbf{R}$  denotes the lattice sites,  $\mathbf{d}$  denotes the two unit vectors  $\mathbf{d}_x$  and  $\mathbf{d}_y$  which connects the nearest neighbor sites in the  $x$  and  $y$  directions respectively.  $\alpha, \beta$  are the spin indexes.  $t$  is the hopping amplitude,  $\mu$  is the chemical potential,  $U_R$  is the Rashba coupling strength,  $V_x$  is the Zeeman energy caused

by a magnetic field along the wire in the x-direction.  $\Delta$  is the superconducting pairing amplitude and  $V_{\text{imp}}(\mathbf{R})$  is the on-site random impurity which is randomly distributed in the range  $[-w/2, w/2]$  at each site. In this work, we set  $V_x = 2\Delta$  such that the superconducting wire can support MF end states by tuning the chemical potential.

The parameters in the tight-binding model are chosen to match the corresponding values in a recent experiment done in Ref.[13]. Here,  $\Delta = 250\mu\text{eV}$ ,  $t = 25\Delta$  and  $U_R = 2.5\Delta$ . The dimensions of the wire are  $N_x a \approx 1\mu\text{m}$  and  $N_y a \approx 100\text{nm}$  which is about twice the superconducting coherence length  $\xi_0$  of the system. The length of the wire chosen is about half the length of the experimental value in Ref.[8]. Due to the short length of the wire, as shown in Fig.2a, the energy versus chemical potential plot exhibits oscillatory behaviour in the topologically non-trivial regime [19, 26] instead of staying at zero energy as the two MF end states can couple to each other.

To study the current-current correlation mediated by the MF end states, two semi-infinite normal leads are attached to the two ends of the TS as shown in Fig.1a. The two normal leads are described by Eq.1 by setting  $\Delta$  to zero. The tunnelling barriers are simulated by the reduced hopping amplitudes  $t_{LC} = t_{RC} = 0.3t$  between the leads and the superconductor where  $t_{LC}$  ( $t_{RC}$ ) denotes the hopping amplitude from the left (right) lead to the TS.

We use the recursive Green's function method to calculate the scattering matrix of the model [21] where the scattering matrix is related to the Green's functions by

$$S_{ij}^{\alpha\beta} = -\delta_{i,j}\delta_{\alpha,\beta} + i[\Gamma_i^\alpha]^{1/2} * G^r * [\Gamma_j^\beta]^{1/2}. \quad (2)$$

Here,  $S_{ij}^{\alpha\beta}$  is an element of the scattering matrix which denotes the scattering amplitude of a  $\beta$  particle from lead  $j$  to an  $\alpha$  particle in lead  $i$ .  $i, j = 1$  or  $2$ . 1 and 2 denote the left and the right lead respectively.  $\alpha, \beta \in \{e, h\}$  denotes the electron (e) or hole (h) channels.  $G^r$  is the retarded Green's function of the superconducting wire.  $\Gamma_i^\alpha = i[(\Sigma_i^\alpha)^r - (\Sigma_i^\alpha)^a]$ , where  $(\Sigma_i^\alpha)^{r(a)}$  is the  $\alpha$  particle retarded (advanced) self-energy of lead  $i$ .

With the scattering matrix, the average current  $\bar{I}$ , the differential shot noise  $P_{ij}$  and shot noise  $C_{ij}$  can be calculated as:[22, 23]

$$\begin{aligned} \bar{I} &= \frac{e}{h} \int_0^{eV} \sum_{j,\alpha} \text{Tr}[I - \text{sgn}(\alpha) S_{ij}^{e\alpha}(E)^\dagger S_{ij}^{e\alpha}(E)] dE, \\ P_{ij} &= \sum_{\alpha, k\beta \neq l\beta'} \text{sgn}(\alpha) \text{Tr}[S_{il}^{e\beta'}(E)^\dagger S_{ik}^{e\beta}(E) S_{jk}^{\alpha\beta}(E)^\dagger S_{jl}^{\alpha\beta'}(E)], \\ C_{ij} &= \frac{2e^2}{h} \int_0^{eV} P_{ij}(E) dE, \end{aligned} \quad (3)$$

where  $\text{sgn}(\alpha) = 1$  if  $\alpha = e$  and  $\text{sgn}(\alpha) = -1$  if  $\alpha = h$ . In this work, we set the chemical potential of the two normal leads to be the same and the voltage bias between the leads and the superconductor to be  $V$ . Physically,  $C_{ij} = \int_{-\infty}^{+\infty} \delta I_i(0) \delta I_j(t) dt$  measures the current fluctuation of leads  $i$  and  $j$ , where  $\delta I_i = I_i(t) - \bar{I}_i$  denotes the deviation of the current at time  $t$  with respect to the average current  $\bar{I}_i$ . At low temperatures with  $T \ll eV/k_B$ , the current fluctuation is

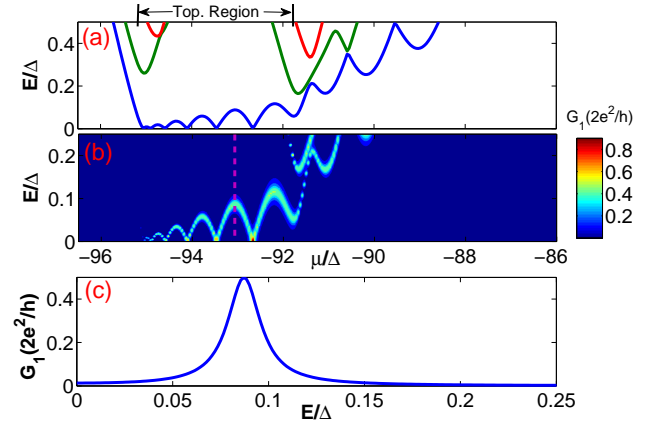


FIG. 2: (a) The energy spectrum of a quasi-1D wire with  $N_x a = 1\mu\text{m}$ . The topological region is indicated above. (b) Contour plot of differential conductance  $G_1$  of the left lead as a function of chemical potential and electron incident energy  $E$ . The conductance shows an oscillatory behavior in the topological regime. (c)  $G_1$  versus incident energy at a fixed chemical potential denoted by the red dashed line in (b). The height of the peak at  $E = E_M$  is  $\frac{2e^2}{h} \frac{t_1^2}{t_1^2 + t_2^2}$ .

dominated by the shot noise [24] and thus we simply denote  $C_{ij}$  as the shot noise and  $P_{ij}$  as the differential shot noise.

When the superconducting wire is in the topological regime with only one transverse subband occupied and two MFs appear as end states, we expect the transport properties of the N/TS/N junction at  $eV \ll \Delta$  to be qualitatively described by the effective Hamiltonian  $H_{eff} = H_L + H_M + H_T$ , where

$$\begin{aligned} H_L &= -iv_f \sum_{\kappa \in L/R} \int_{-\infty}^{+\infty} \psi_\kappa^\dagger(x) \partial_x \psi_\kappa(x) dx, \\ H_M &= iE_M \gamma_L \gamma_R \\ H_T &= -i[t_L \gamma_L (\psi_L^\dagger(0) + \psi_L(0)) + t_R \gamma_R (\psi_R^\dagger(0) + \psi_R(0))]. \end{aligned} \quad (4)$$

In Eq.4,  $\psi_{L/R}$  denotes a fermion operator of the left (right) normal lead.  $v_f$  is the corresponding Fermi velocity.  $E_M$  is the coupling strength between the two MF end states and  $\gamma_L$  and  $\gamma_R$ . The coupling strengths between the normal leads and the TS are denoted by  $t_L$  and  $t_R$  respectively. This model was first introduced in Refs.[24, 25] and the scattering matrix of the Hamiltonian can be found using the equation of motion approach [11]. With the scattering matrix, the current and shot noise can be calculated using Eq.3. In the following, we show that the numerical results of the tight-binding model in the first topological regime, where only one transverse subband of the wire is occupied, and the results from the effective Hamiltonian model agree well with each other. However, the effective model  $H_{eff}$  does not apply to the wires with more than one occupied transverse subband. The multi-channel regime and the effect of disorder are studied based on the lattice Green's function approach.

**Current**— In this section, we focus on the tunnelling current near the topological regime where only one transverse sub-band is occupied. However, due to the short wire geometry, the MFs at the two ends couple to each

other quite strongly. Due to the oscillatory nature of the MF wavefunctions, the coupling strength of the MFs oscillates and the resulting coupling energy oscillates as  $E_M \approx \frac{\hbar^2 k_F}{m^* \xi_0} e^{-2N_x a / \xi_0} \cos(k_F N_x)$ , where  $k_F$  is the Fermi momentum which is a function of chemical potential and magnetic field [26]. The energy spectrum of the TS is shown in Fig.2a. The topological regime marked out in Fig.2a is determined in the long wire limit where zero energy modes appear. As the chemical potential increases and a second transverse subband is occupied, the TS becomes topologically trivial.

To study the MF end states, we calculate the differential conductance  $d\bar{I}_1/dV$  using Eq.3. The contour plot of the differential conductance  $G_1 = d\bar{I}_1/dV$  as a function of electron incident energy  $E = eV$  and the chemical potential is shown in Fig.2b. As expected, the MFs manifest themselves by inducing conductance peaks. However, when the two MFs couple to each other and  $E_M \gg t_1^2, t_2^2$ , the height of the differential conductance peak is reduced to  $G_1(E_M) = d\bar{I}_1/dV|_{eV=E_M} \approx \frac{2e^2}{h} \frac{t_1^2}{t_1^2 + t_2^2}$  from the usual  $\frac{2e^2}{h}$  for the one lead geometry. Here,  $t_1 = \sqrt{\frac{2}{v_f}} t_L$  ( $t_2 = \sqrt{\frac{2}{v_f}} t_R$ ) is the effective coupling strength between the left (right) normal lead and the TS.

Another interesting point for tunnelling into a TS with two strongly coupled MFs is that at low incident energy  $E \ll E_M$ , the differential conductance  $G_1(E) \approx \frac{2e^2}{h} \frac{t_1^2 t_2^2}{E_M^2}$  depends on the product of  $t_1$  and  $t_2$ . This means that an electron from a normal lead cannot tunnel into the TS unless a second normal lead is coupled to the TS. This is a manifestation of the fact that local Andreev reflection processes are suppressed and the current is purely caused by crossed Andreev reflection processes in this regime. In other words, the strongly coupled MF end states drastically change the local and non-local transport properties of the N/TS/N junction. As it is shown below, the measurements of the differential shot noise and shot noise can be used to probe the topological regime unambiguously.

**Differential Shot Noise**— The contour plots of the differential shot noise  $P_{11}(E)$  and  $P_{12}(E)$  defined in Eq.3 are shown in Fig.3a and Fig.3b, respectively. In Fig.3,  $P_{11}$  and  $P_{12}$  at energy  $E$  are normalized by the differential conductance  $G_1(E)$  and the average differential conductance  $\bar{G}(E) = \frac{1}{2}(G_1 + G_2)$  respectively. The ratio  $F(E) = P_{11}(E)/G_1(E)$  is the Fano factor for electrons at incident energy  $E$ . At weak tunnelling limit, the Fano factor gives the value of the tunnelling charge at each tunnelling event. From Fig.3a and Fig.3e, it is clear that the Fano factor at  $E = 0$  is the electron charge  $e$  in the topological regime. Similarly, the Fano factor for the right lead is  $P_{22}(E = 0)/G_2(E = 0) = e$ . This indicates that for each tunnelling event, each normal lead contributes one electron in the tunnelling process. Moreover, it is evident from Fig.3b and Fig.3e that  $P_{12}(E = 0)/\bar{G} = e$ , where  $P_{12}$  is the current-current correlation of two *different* leads. As pointed out in Ref.[24], the cross correlator  $P_{12}$  is bound by the relation  $2|P_{12}| \leq P_{11} + P_{22}$  for any stochastic processes. At  $E = 0$ , we have  $2|P_{12}(E)| =$

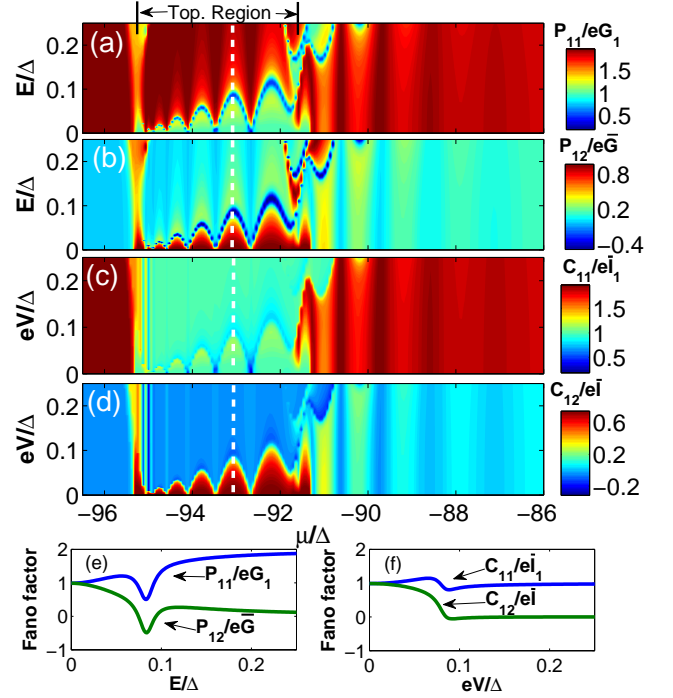


FIG. 3: (a) Contour plot of Fano factor  $P_{11}/eG_1$  for electrons with incident energy  $E$  at chemical potential  $\mu$ . (b) Contour plot of the crossed Fano factor  $P_{12}/e\bar{G}$ . (c) Contour plot of Fano factor  $C_{11}/e\bar{I}_1$  as a function of voltage bias  $eV$  and chemical potential. (d) Contour plot of crossed Fano factor  $C_{12}/e\bar{I}$ . (e) The Fano factors  $P_{11}/eG_1$  and  $P_{12}/e\bar{G}$  as a function of incident energy  $E$  at a fixed chemical potential denoted by the dashed lines in (a) and (b). (f) The Fano factors  $C_{11}/e\bar{I}_1$  and  $C_{12}/e\bar{I}$  as a function of voltage bias at fixed chemical potential denoted by the dashed lines in (c) and (d).

$$P_{11}(E) + P_{22}(E).$$

This indicates that the two leads are perfectly correlated with each other such that a Cooper pair is injected into the superconductor at each tunnelling event (as depicted in Fig.1c). This is in sharp contrast to the topologically trivial regime as shown in Fig.3a in which local Andreev reflection processes (as depicted in Fig.1b) dominate and the Fano factor for each lead is  $2e$  instead. The tunnelling currents of the two leads are only weakly correlated in the absence of MFs.

Away from  $E = 0$ , we see that the Fano factor in the topological regime is strongly energy dependent. It is also shown in Fig.3a and Fig.3e that the Fano factor  $P_{11}(E)/G_1(E)$  reaches a minimum value of  $\frac{t_2^2}{t_1^2 + t_2^2}e$  at  $E = E_M$  when the tunnelling conductance is maximum. For  $E \gg E_M$ , local Andreev reflection processes dominate and the Fano factor approaches  $2e$ . On the contrary, the shot noise of  $2e$  in the trivial regime is insensitive to the energy of the incident electrons as long as the energy is much smaller than the first Andreev bound state energy of the wire. Since the Fano factor behaves very differently in the topologically trivial and non-trivial regimes, it can be used to determine the topological regime unambiguously. As it is shown in Fig.2a,  $E_M$  is about  $0.1\Delta$  for a realistic wire and it can be even larger for a shorter

wire [27]. Therefore, the experimental measurements of the energy dependence of the Fano factor is highly feasible.

It is important to note that the cross correlator  $P_{12}$  also exhibits strong energy dependence in the topological regime. As shown in Fig.3b and Fig.3e,  $P_{12}/e\bar{G} \approx \frac{E_M^2}{E_M^2 + t_1^2 t_2^2} \approx 1$  for  $E \ll E_M$ . At  $E = E_M$ ,  $P_{12}/e\bar{G} \approx -\frac{2t_1^2 t_2^2}{(t_1^2 + t_2^2)^2}$ . At  $E \gg E_M$ , local Andreev reflections dominate at each lead and the correlations between the two leads drop to zero eventually. On the other hand, in the absence of MFs outside of the topological regime,  $P_{12}$  drops to zero quickly, independent of the incident energy. Therefore, the measurement of  $P_{12}$  provides another way to probe the topologically non-trivial regime.

**Shot Noise**— In this section, we study the shot noise  $C_{ij}$ , which is the integration of the differential shot noise over the incident energy of the electrons as defined in Eq.3. The contour plots of  $C_{11}$  and  $C_{12}$ , normalized by  $\bar{I}_1$  and  $\bar{I} = \frac{1}{2}(\bar{I}_1 + \bar{I}_2)$  respectively, as a function of chemical potential and voltage bias are shown in Fig.3c and Fig.3d. The Fano factor  $C_{ii}/\bar{I}_i$  gives the charge leaving lead  $i$  at each tunnelling event. As expected, in the crossed Andreev reflection regime with  $E \ll E_M$ ,  $C_{ii}/\bar{I}_i = e$ . In this case, the two leads are perfectly correlated as  $C_{12}/\bar{I} = e$ .

Outside of the topological regime,  $C_{ii}/\bar{I}_i \approx 2e$  as local Andreev reflection processes dominate. Moreover, the cross correlation between the two leads  $C_{12}$  is significant only when the incident energy of electrons satisfies  $E \ll E_M$  in the topological regime as shown in Fig.3d.

**Disorder effect**— The observation of the ZBCPs in recent tunnelling experiments is an important step in the search for MFs in solid state systems [8–10]. However, as argued in Ref.[13], fermionic end states formed by two MF end states in the topologically trivial regime can also induce ZBCPs in the presence of disorder. Therefore, it is important to distinguish the fermionic end states from the true MF end states. In this section, we show that the shot noise caused by a localized fermionic end state and the shot noise caused by a non-local fermionic state formed by two spatially separated MF end states are different.

On-site random disorder with strength  $\omega = 20\Delta$  is added to the superconducting wire. The contour plots of the conductance  $G_1$  and  $G_2$  are shown in Fig.4a and Fig.4b respectively. It is important to note that in the topologically trivial regime where two transverse subbands of the wire are occupied, a fermionic end state which has energy close to zero is induced by disorder at  $\mu \approx -84\Delta$ . The ground state wavefunction at  $\mu = -84.6\Delta$  is shown in Fig.4f and it is evident that the ground state is localized at the left end of the wire. As expected, this zero energy fermionic end state induces a strong conductance peak for the left normal lead-superconductor junction. Moreover, the energy of the fermionic state oscillates as a function of chemical potential and it is difficult to distinguish this fermionic state from a true MF end state by measuring the conductance alone.

However, since the fermionic state at  $\mu \approx -84\Delta$  is a localized state, the cross current-current correlation  $P_{12}/\bar{G}$  in-

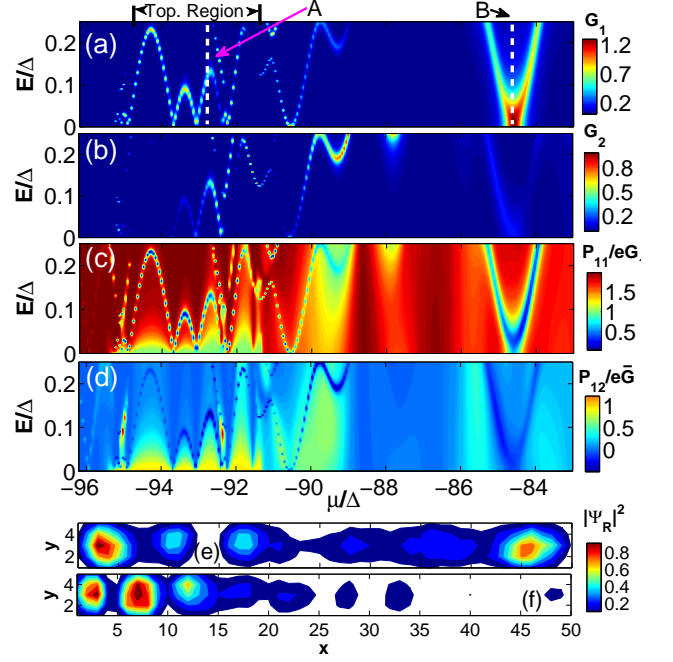


FIG. 4: Random disorder with  $\omega = 20\Delta$  is present for all the figures. (a) and (b): The contour plots of the conductance  $G_1$  and  $G_2$ , respectively. (c) and (d): The Fano factors  $P_{11}/e\bar{I}_1$  and  $P_{12}/e\bar{I}$ , respectively. (e) The ground state wavefunction magnitude  $|\Psi_R|^2$  in the topological regime with  $\mu = -92.7\Delta$  (indicated by dashed line A in (a)). The dimensions of the wire is  $N_x = 50a$  and  $N_y = 5a$ . (f) The ground state wavefunction magnitude in the trivial regime with  $\mu = -84.6\Delta$  (indicated by dashed line B in (a)).

duced by this state is small as shown in Fig.4d. On the contrary,  $P_{12}/\bar{G}$  is close to 1 in the topological regime. Moreover, the Fano factor  $P_{11}/eG_1$  at  $E \approx 0$  is close to 1 only in the topological regime which indicates that crossed Andreev reflection processes dominate. The ground state wavefunction in the topological regime at  $\mu = -92.7\Delta$  is shown in Fig.4e. It is evident that this fermionic end state, which can mediate crossed Andreev reflections, is a non-local fermionic state formed by two MF end states.

**Conclusion** — We show that the measurements of current and shot noise in a N/TS/N junction can be used to determine the topological regimes of the superconducting wire with MF end states unambiguously. Particularly, the shot noise can be used to distinguish the fermionic end states from true MF end states even in the presence of disorder.

**Acknowledgement**— We thank H. Jiang, P.A. Lee, X.J. Liu, A.C. Potter, Q.F. Sun and especially M. Heiblum for insightful discussions. KTL and JL thank the support of HKRGC through Grant 605512 and HKUST3/CRF09. FCZ thanks the support of RGC HKU707211 and AOE/P-04/08.

\* Correspondence address to: jliuphy@hku.hk

† Correspondence address to: phlaw@ust.hk



- [1] J.D. Sau, R.M. Lutchyn, S. Tewari, and S. Das Sarma, Phys. Rev. Lett. **104**, 040502 (2010).
- [2] S. Fujimoto, Phys. Rev. B. **77**, 220501(R) (2008).
- [3] M. Sato, Y. Takahashi, and S. Fujimoto, Phys. Rev. B **82**,134521 (2010).
- [4] J. Alicea, Phys. Rev. B **81**, 125318 (2010).
- [5] R.M. Lutchyn, J.D. Sau, and S. Das Sarma, Phys. Rev. Lett. **105**, 077001 (2010).
- [6] Y. Oreg, G. Refael, and F. von Oppen, Phys. Rev. Lett. **105**, 177002 (2010).
- [7] A. C. Potter and P. A. Lee, Phys. Rev. B **83**, 094525 (2011).
- [8] V. Mourik, K. Zuo, S.M. Frolov, S.R. Plissard, E.P.A.M. Bakkers, and L.P. Kouwenhoven, Science **336**, 1003 (2012).
- [9] M. T. Deng, C.L. Yu, G.Y. Huang, M. Larsson, P. Caroff, H.Q. Xu, arXiv: 1204.4130 (2012).
- [10] A. Das, Y. Ronen, Y. Most, Y. Oreg, M. Heiblum, H.Shtrikman, Nature Physics **8**, 887 (2012).
- [11] K.T. Law, P.A. Lee, and T.K. Ng Phys. Rev. Lett. **103**,237001 (2009).
- [12] M. Wimmer, A.R. Akhmerov, J.P. Dahlhaus, C.W.J. Beenakker, New J. Phys. **13**, 053016 (2011).
- [13] J. Liu, A. C. Potter, K.T. Law, P. A. Lee, Phys. Rev. Lett. **109**, 267002 (2012).
- [14] D. Bagrets, A. Altland, arXiv:1206.0434 (2012).
- [15] D. I. Pikulin, J. P. Dahlhaus, M. Wimmer, H. Schomerus, C. W. J. Beenakker, arXiv:1206.6687 (2012).
- [16] G. Kells, D. Meidan, and P. W. Brouwer, Phys. Rev. B **85**, 060507(R) (2012).
- [17] S. Tewari, T. D. Stanescu, J. D. Sau, and S. Das Sarma, Phys. Rev. B **86**, 024504 (2012).
- [18] F. Pientka, G. Kells, A. Romito, P. W. Brouwer, F. von Oppen, arXiv:1206.0723.
- [19] D. Rainis, L. Trifunovic, J. Klinovaja, D. Loss arXiv:1207.5907.
- [20] A. Das, Y. Ronen, M. Heiblum, D. Mahalu, A. V. Kretinin, H. Shtrikman, Nat. Commun. 3:1165 doi: 10.1038/ncomms2169 (2012).
- [21] P.A. Lee and D.S. Fisher, Phys. Rev. Lett. **47**, 882 (1981); D.S. Fisher and P.A. Lee Phys. Rev. B **23**, 6851 (1981).
- [22] Q.F. Sun and X. C. Xie, J. Phys. Condens. Matter. **21**, 344204 (2009).
- [23] M. P. Anantram and S. Datta, Physical Review B, **53**, 16390 (1996).
- [24] J. Nilsson, A. R. Akhmerov, and C. W. J. Beenakker, Phys. Rev. Lett. **101**,120403 (2008).
- [25] C. J. Bolech and E. Demler, Phys. Rev. Lett. **98**, 237002 (2007).
- [26] S. Das Sarma, J. D. Sau, T. D. Stanescu, arXiv:1211.0539.
- [27] However, the wire cannot be much shorter than the coherence length. If the wire is too short, the cross Andreev reflection amplitude can be significant even in the absence of MFs.